ACS APPLIED MATERIALS & INTERFACES

Research Article

www.acsami.org

Interfacial Chemical Composition and Molecular Order in Organic Photovoltaic Blend Thin Films Probed by Surface-Enhanced Raman Spectroscopy

Joseph Razzell-Hollis,[†] Quentin Thiburce,[†] Wing C. Tsoi,[†,‡] and Ji-Seon Kim*[,†]

[†]Department of Physics and Center for Plastic Electronics, Imperial College London, London SW7 2AZ, United Kingdom

[‡]SPECIFIC, College of Engineering, Swansea University, Swansea SA1 8EN, United Kingdom

Supporting Information

ABSTRACT: Organic electronic devices invariably involve transfer of charge carriers between the organic layer and at least one metal electrode, and they are sensitive to the local properties of the organic film at those interfaces. Here, we demonstrate a new approach for using an advanced technique called surface-enhanced raman spectroscopy (SERS) to quantitatively probe interfacial properties relevant to charge injection/extraction. Exploiting the evanescent electric field generated by a ∼7 nm thick layer of evaporated silver, Raman scattering from nearby molecules is enhanced by factors of 10−1000× and limited by a distance dependence with a measured decay length of only 7.6 nm. When applied to the study of an all-polymer 1:1 blend of P3HT and F8TBT used in organic solar cells, we find that the as-cast film is morphologically suited to charge extraction in inverted devices, with a top (anode) interface very rich in hole-transporting P3HT (74.5%) and a bottom (cathode) interface slightly rich in electron-transporting F8TBT (55%). While conventional, uninverted P3HT:F8TBT devices are reported to perform poorly compared to inverted devices, their efficiency can be improved by thermal annealing but only after evaporation of a metallic top electrode. This is explained by changes in composition at the top interface: annealing prior to silver evaporation leads to a greater P3HT concentration at the top interface to 83.3%, exaggerating the original distribution that favored inverted devices, while postevaporation annealing increases the concentration of F8TBT at the top interface to 34.8%, aiding the extraction of electrons in a conventional device. By nondestructively probing buried interfaces, SERS is a powerful tool for understanding the performance of organic electronic devices.

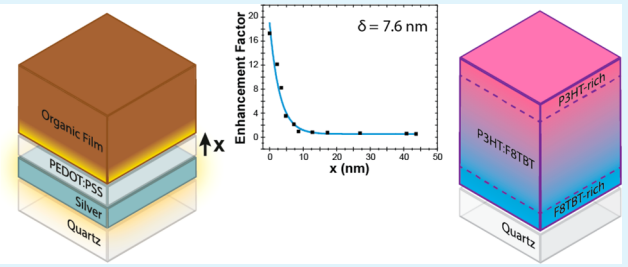

KEYWORDS: *organic electronics, SERS, interfacial properties, charge extraction, conjugated polymers*

INTRODUCTION

Organic photovoltaics (OPVs) and organic light-emitting diodes (OLEDs) are part of a promising new generation of electronic devices that use an active layer composed of conjugated polymer and/or semiconducting small molecules instead of inorganic materials, with the potential for low-cost fabrication via solution processes such as roll-to-roll printing.[1−4] The performance of organic devices has improved significantly in recent years, with OPVs approaching power conversion efficiencies of 12%,[5] due, in part, to the development of novel polymers with a broad range of optoelectronic properties. However, there are also complex relationships between the morphology of the photoactive layer and the electronic processes that determine efficiency, and understanding these relationships is essential to the optimization of device design so that optimum device performance can be quickly obtained from newly developed polymers.[6,7]

The investigation and optimization of morphology in OPV thin films has tended to focus on the donor:acceptor blend that acts as the active layer and, specifically, the effects of bulk properties and lateral organization of the blend on key electronic processes like exciton dissociation, charge generation, and charge transport.[7−9] However, for vertically stacked devices like OPVs and OLEDs, where the active layer (∼100 nm) is sandwiched between two electrodes, charge extraction/injection will be extremely dependent on the properties of the film/electrode interface.[10−14] The formation of ultrathin interfacial layers with a chemical composition, organization, and energetics distinct from the bulk of the blend may have a disproportionate effect on overall device performance, and consequently, it is extremely important to characterize the local properties at both the top and bottom interfaces of the blend.

The study of interfacial properties in thin films, particularly with respect to chemical composition and molecular order, is a tricky one, as surface sensitive techniques cannot probe buried interfaces (i.e., substrate/film) without cleaving or otherwise damaging the sample.[4,15] Additionally, typical film thicknesses used in OPVs are much smaller than the vertical resolution of

Received: September 23, 2016
Accepted: October 27, 2016
Published: October 27, 2016

DOI: 10.1021/acsami.6b12124
ACS Appl. Mater. Interfaces 2016, 8, 31469−31481

most microscopy techniques (~μm), which therefore cannot distinguish interfacial properties from those of the bulk film. An altogether more promising technique for the study of interfacial properties is surface-enhanced raman spectroscopy (SERS), which exploits the localized electric field generated by surface plasmons on metallic nanostructures to selectively enhance Raman scattering by up to $10^{11}\times$ from only those molecules within a few nanometers of a metal surface.[16−18] Surface enhancement has so far attracted greater interest as a method for increasing PCE through the enhancement of local absorption and light-scattering by embedding metal nanoparticles in the active layer. However, by combining the short-range of the enhancement effect with the sensitivity of conventional Raman spectroscopy to relevant material properties such as chemical structure and conformation,[6,7,19] it is possible to use SERS to probe the composition and morphology of metal/organic interfaces within ~100 nm thick organic thin films. The application of SERS to study organic semiconductors and thin films is relatively novel[20−22] and has been limited in part by the following problems: (1) disruption of thin film morphology by the introduction of metallic nanostructures, (2) difficulty in estimating the <10 nm decay length of the enhancement effect, and (3) that the SERS enhancement factor (EF) can only be calculated when the number/density of molecules is known.

In this article, we will detail a new methodology for applying SERS to the study of interfacial properties in organic thin films. This will include how to fabricate metallic substrates appropriate for probing morphology without disrupting it, defining enhancement in the complex situation of an optically thin polymer film, accounting for several factors that influence both Raman and SERS intensities in these measurements and eventually obtaining a quantitative description of interfacial composition. Finally, we will demonstrate how SERS can be used to develop a better understanding of the relationships between vertical morphology and device performance for an all-polymer OPV with an active layer containing a blend of poly(3-hexylthiophene) (P3HT) and poly((9,9-dioctylfluorene)-2,7-diyl-*alt*-[4,7-bis(3-hexylthien-5-yl)-2,1,3-benzothiadiazole]-2′,2″-diyl) (F8TBT). P3HT:F8TBT blends have a reported efficiency of ~2%, which is only achieved when the blend is thermally annealed *after* evaporation of a metallic capping electrode.[23] This suggests there is an important morphological change taking place at the top interface in the presence of the metal and makes the P3HT:F8TBT blend an ideal example for demonstrating the use of SERS.

EXPERIMENTAL METHODS

Silver Layer Deposition. Thermal evaporation was used to deposit a ~7 nm thick layer of Ag (Sigma-Aldrich, ~ 99% purity) onto either cleaned quartz (Spectrosil, UCQ Ltd.) or organic films, depending on the sample configuration (Q/Ag/polymer or Q/polymer/Ag). Evaporation was done at a pressure of $<1\times10^{-6}$ mbar and a rate of ~0.15 Å/s, through a 6-pixel mask (pixel area 4.5 mm^2) such that each sample had regions of Ag for SERS measurements and regions without Ag for conventional Raman. Oxidation of the metal layer (or any organic layers underneath) was minimized by using an evaporator situated in a nitrogen glovebox system.

Organic Film Preparation. The organic layers being probed by SERS were made using P3HT (Merck Chemicals, MW = 31 kDa, $Đ$ = 2.0, RR = 94%); F8TBT (supplied by Cambridge Display Technologies Ltd.) and rhodamine-6G (Sigma-Aldrich). P3HT and F8TBT were dissolved in *p*-xylene at 70 °C to make up standard 20 mg/mL solutions for each neat material and a blend solution with a 1:1 weight ratio.[23] Films were then deposited from solution via spin-coating at 2000 rpm for 120 s, and film thicknesses varied by diluting the standard solutions. Spacer layers were made from an aqueous solution of PEDOT:PSS (Heraeus), which was spin-coated at 4000 rpm for 90 s. Spacer thickness was varied from 44 to 2.2 nm by diluting the solution from its as-purchased concentration of 6%. Rhodamine-6G was dissolved in H_2O at a concentration of 2.1×10^{-7} mol/L in order to produce a monolayer when 100 μL was drop-cast onto a 12 × 12 mm substrate. Thermal annealing was done in a nitrogen glovebox at 140 °C for 10 min.

Film Characterization. AFM scans were done using a Park NX10 microscope, while optical transmittance and reflectance measurements were done using a Shimadzu UV-2600 spectrophotometer with an integrating sphere attachment, and absorption was calculated from transmittance using the Beer−Lambert law. Each Q/Ag substrate was measured both right-way-up (with the Ag layer facing the incident light) and upside-down (with the Ag layer facing away). Raman and SERS measurements were done using a Renishaw inVia microscope with a 50× objective in a backscattering configuration. The excitation source was a 488 nm (Ar ion) laser, and spectra were taken using a laser power of 0.45 mW and an acquisition time of 30 s (0.9 mW and 60 s for Rho-6G). Laser intensities and acquisition times were the same for both Raman and SERS, and three measurements of each were taken in different locations to obtain average spectra for each sample. To reduce laser-induced photodegradation, samples were measured in a Linkam thermal stage under N_2 purging, and the laser spot was defocused to ~20 μm. Organic film thicknesses were measured using a Dektak profilometer; for films of <10 nm thickness, AFM was used for greater accuracy.

DFT Simulations. P3HT and F8TBT oligomers were simulated by the Gaussian 09 software package, using the B3LYP 6-31G(d,p) basis set. Molecular structures were first optimized in the gas phase, and then theoretical Raman spectra were calculated. Raman shifts were adjusted using an empirical 0.960 scaling factor according to the 6-31G(d,p) basis set. Alkyl side-chains were reduced to methyl groups to aid computation time.

RESULTS AND DISCUSSION

In traditional SERS experiments, the surface enhancement effect is produced by a layer of either silver or gold, as these metals are known to achieve the strongest plasmon resonance at visible wavelengths, while the analyte is typically a molecular monolayer adsorbed to the metal surface or a dilute solution.[18,24] However, as we intend to investigate the properties of relatively thick organic films used in electronic devices, we must develop an appropriate methodology for achieving SERS within that regime. To this end, we prepared samples of organic thin films on quartz ("Q") substrates with two configurations, Q/Ag/organic and Q/organic/Ag, to selectively probe either the bottom or top interface of the organic film (referred to from now on as bottom-contact and top-contact, respectively). Silver was chosen as it has a plasmon resonance close to our desired excitation wavelength, 488 nm (vide infra), and was prepared using a 6-pixel mask to ensure that each sample would have both regions without Ag (for normal Raman measurements) and regions with Ag (for SERS measurements).

SERS substrates are usually prepared by electrochemical etching of solid metal, deposition of metallic nanoparticles (10−100 nm in diameter) or the fabrication of periodic surface structures,[18,24] but all have surface height variations and feature sizes equal to or larger than the thickness of organic films typically used in OPVs (~100 nm) and thus will interfere with the morphology we wish to probe. In order to avoid this, we instead used thermal evaporation to deposit a relatively smooth

DOI: 10.1021/acsami.6b12124
ACS Appl. Mater. Interfaces 2016, 8, 31469−31481

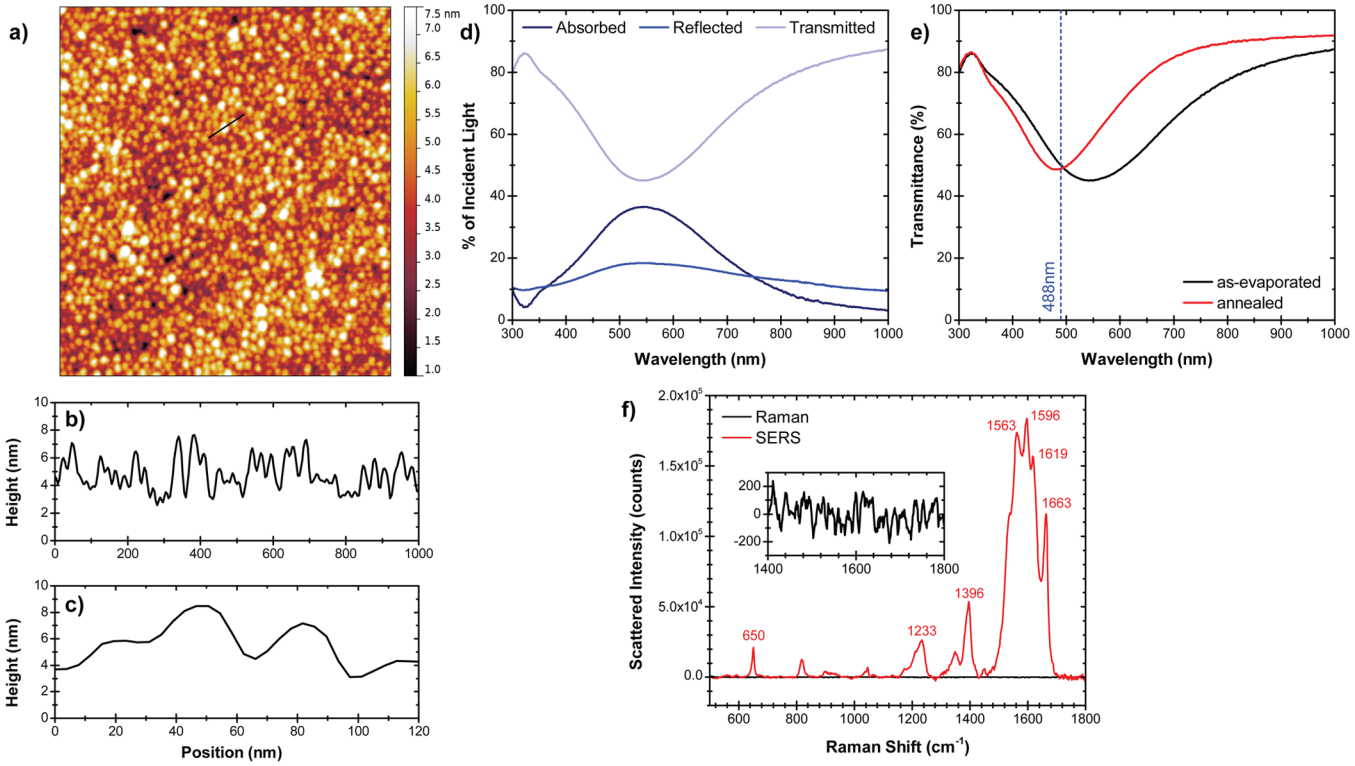

Figure 1. (a) 1 × 1 μm AFM image of an evaporated Ag surface used for SERS and (b,c) surface profiles measured by AFM. (d) Absorptance, reflectance, and transmittance spectra (in %) for an Ag layer on quartz, (e) transmittance spectra before and after thermal annealing at 140 °C. (f) Raman and SERS spectra for a monolayer of Rho-6G drop-cast onto Ag, inset: a close-up of the Raman spectrum, showing only random noise and no detectable peaks.

thin layer of metal, ∼7 nm thick, onto the desired substrate. Employing a slow evaporation rate of ∼0.15 Å/s led to a nanoparticle-like surface of circular features approximately 25−50 nm in width and 2−6 nm in height (see Figure 1a−c), and a surface roughness of only ∼1 nm, comparable to that of the indium tin oxide (ITO) electrodes used in device fabrication. Consequently, we expect that the Ag layer will have a minimal effect on thin film morphology.

The evaporated Ag layer on quartz (Q/Ag) exhibited a strong plasmon resonance in its optical spectra (Figure 1d), appearing as a reduction in transmittance due to greater absorbance and reflectance when incident light is strongly coupled to surface plasmon modes. The resonance wavelength, λ_{LSP}, was estimated from the maximum to be ∼540 nm, though the resonance peak was very broad, with a full width at half-maximum (fwhm) of 355 nm. This led to a resonance quality factor Q of 1.5, defined by the ratio of λ_{LSP} to fwhm, which can be used to indicate uniformity of the metallic nanostructure. The measured factor, 1.5, is significantly lower than values reported in the literature and can be attributed to the nonperiodic nature of the evaporated surface compared to more uniform SERS substrates such as nanoparticles, which can produce sharply defined resonance peaks with fwhm of <10 nm and $Q > 40$.[24] However, the resonance peak in Figure 1 is considered ideal for our experiments, being highly resonant across the visible spectrum and having a λ_{LSP} close to our chosen excitation wavelength, 488 nm.

Thermal annealing was found to have an effect on the optical properties of the Ag layer: after 10 min of annealing at 140 °C, there was a 59 nm blue-shift in λ_{LSP}, from 540 to 482 nm, and a marked reduction in fwhm, from 355 to 254 nm, leading to an improvement in quality factor Q from 1.5 to 1.9. This can be explained by a reconfiguring of the surface structure, revealed by AFM as a reduction in feature size and surface roughness (not shown). The extinction at 488 nm was unaffected, and so we expect to achieve a similar degree of resonance from both as-evaporated and annealed substrates.

A significant issue for SERS substrates fabricated using thermal evaporation is the inherent batch-to-batch variation that arises from small fluctuations in evaporation rate and differences in pressure and temperature, all of which influence how the atoms are deposited. To account for these variations, each batch of evaporated substrates was characterized separately using AFM (to find feature sizes and surface roughness) and optical spectroscopy (to find the plasmon resonance and optical density). However, across seven batches, we found relatively little variation in optical extinction in the 488−535 nm range critical to our measurements (see Supporting Information), and the variation was accounted for through the calculation of an optical correction factor for each batch, as shown in the next section.

A key parameter of SERS experimentation is the enhancement factor (EF), which is the ratio of intensities obtained with and without surface enhancement, I_{SERS}/I_{RS}. This basic definition fails to account for several factors that influence the two intensities, particularly the large difference in number of molecules contributing to each value. In a typical application of SERS, the analyte is either in solution or adsorbed to the metal surface as a monolayer. This neatly avoids any concerns about the distance dependence of enhancement, and the numbers of molecules within the focal volume that are involved in Raman or SERS scattering are well-defined by concentration

DOI: 10.1021/acsami.6b12124
ACS Appl. Mater. Interfaces 2016, 8, 31469−31481

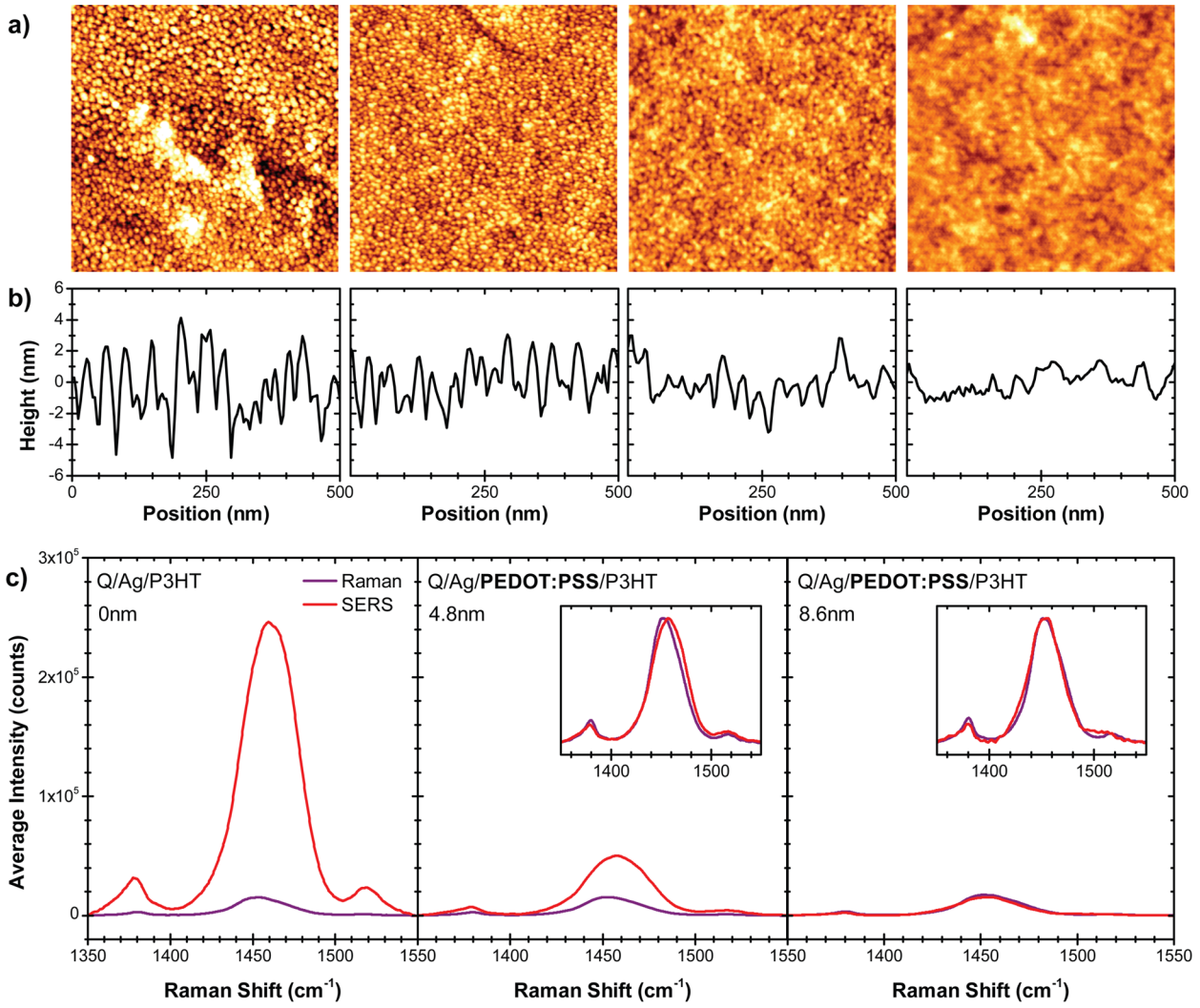

Figure 2. AFM images (a) and surface profiles (b) for four Q/Ag/PEDOT:PSS substrates. From left to right: PEDOT:PSS thicknesses were 0, 4.8, 8.6, and 27 nm. AFM images are 1 × 1 μm with vertical scales of 10 nm. (c) Raman and SERS spectra for films of P3HT on Q/Ag/PEDOT:PSS of different thicknesses, showing the difference in enhancement with increasing separation.

(N_{vol}) and surface coverage (N_{surf}), respectively. This allows for the simple calculation of a more representative single-molecule enhancement factor (smEF) from Raman and SERS intensities, according to the following equation:

$$\text{smEF} = \frac{I_{SERS}}{I_{RS}} \frac{N_{vol}}{N_{surf}} \quad (1)$$

Although this method is not appropriate for organic thin films, it can be used to estimate the magnitude of enhancement produced by the evaporated Ag substrate. To this end, the organic dye molecule Rhodamine-6G was drop-cast onto the Ag surface from sufficiently dilute solution (2.1×10^{-7} mol/L) to ensure formation of no more than a single monolayer. This simplifies the calculation of the single molecule EF immensely, as N_{vol} and N_{surf} become equal, and all molecules can be treated as being at the same distance from the surface. However, Raman scattering from the monolayer proved to be undetectable *except* under SERS conditions (see Figure 1f). The Raman peaks observed under SERS conditions were slightly shifted (± 6 cm^{-1}) with respect to their reported positions, and compared to spectra in the literature, those modes around ~1600 cm^{-1} were markedly stronger.[25] Without a Raman spectrum taken under the same excitation conditions for a direct comparison, it is difficult to assign these variations to any meaningful cause, but it is believed the changes arise from interactions between rhodamine molecules and the metal surface.

Without a known Raman intensity it is not possible to calculate EF, but a lower limit can be estimated from Figure 1f. The Raman background noise was ±200 counts, meaning that any Raman peaks of >400 counts would have been detectable. As the SERS intensity reached 1.83×10^5 counts at 1596 cm^{-1}, the single molecule EF is at least 459× for that particular vibrational mode of rhodamine-6G, and may be much larger. Compared to values reported in the literature for other nanostructured substrates, ~10^6× for roughened Ag and ~10^9× for nanoparticles,[24] we obtain a much weaker enhancement, but this is likely due to the relative smoothness of the evaporated Ag surface compared to those substrates. However, the goal of this work is to exploit the distance dependence of SERS rather than achieve single molecule detection, and thus, low EFs are deemed to be acceptable.

A significant issue in applying SERS to organic thin films is that the ratio N_{bulk}/N_{surf} cannot be calculated. The total number of scattering centers is unknown (for polymers, multiple

DOI: 10.1021/acsami.6b12124
ACS Appl. Mater. Interfaces 2016, 8, 31469−31481

chromophores can exist on a single chain), and the number of scatterers being enhanced is unclear, with no clearly defined monolayers at specific distances. Instead, we propose to describe SERS in organic films by dividing the film into two regions: an interfacial layer, which is close enough to the Ag to experience surface enhancement (where smEF ≫ 1), and the bulk of the film, which does not (smEF = 1). By separating the film into enhanced interface and unenhanced bulk regions, it is possible to calculate an average interfacial enhancement factor EF_{int} that is only dependent on the decay length of the enhancement effect, δ, and is not affected by the actual thickness of the film itself, L. In the absence of the Ag substrate and corresponding enhancement of the interfacial layer, the scattered intensity contributed from each layer, I_{int} and I_{bulk}, will be proportional to the layer thickness, δ and $L - \delta$ respectively. Therefore, the total measured intensity is equal to $I_{int} + I_{bulk}$ under Raman conditions, and EF_{int} $I_{int} + I_{bulk}$ under SERS conditions. With a bit of rearranging (see Supporting Information) it becomes possible to determine the average interfacial EF from the "apparent" EF, determined by the experimentally measured Raman and SERS intensities, as follows:

$$EF_{int} = 1 + \frac{L}{\delta}(EF_{app} - 1) \quad (2)$$

Thus, a reliable, thickness-independent EF can be calculated provided that the decay length δ and film thickness L are known. The calculated EF_{int} value represents the average EF (EF_{app}) that would be obtained from the ratio I_{SERS}/I_{RS} for a film of thickness δ but neatly avoids any impact on morphology that may result from intentionally depositing such ultrathin films. It is important to note that this model only works for films that are thicker than δ, but as reported values of δ vary from 5 to 20 nm,[20,24] the majority of neat films and blends relevant to organic devices are sufficiently thick that this model should be representative.

It is also important to account for the fact that sample configuration can have a significant impact on the measured values of both I_{RS} and I_{SERS}. Bottom-contact (Q/Ag/organic) samples were measured upside down, to avoid direct light absorption by the organic film and ensure a consistent light intensity was incident on the metal layer between different samples, and thus a similar degree of surface enhancement. However, this meant that for both configurations, measured SERS intensities were attenuated due to absorption/reflection by the Ag layer. A correction factor was devised to account for this, based on the transmittance T of the Ag substrate. This factor accounts for both attenuation of incident light at 488 nm, by T (λ_0), and backscattered light at Raman-shifted wavelengths, by T (λ_v). For the substrate characterized in Figure 1, the correction factor varied from 0.2 to 0.3 depending on the Raman shift, meaning that the apparent SERS intensity was ∼1/4 of its "true" value (without attenuation). Additionally, there was a slightly greater correction factor for bottom-contact samples due to added attenuation by the quartz substrate during upside-down measurements (see Supporting Information), and so each spectrum was corrected using the appropriate factor for the evaporation batch and specific sample configuration.

With reliable transmittance-corrected measurements of I_{SERS} and I_{RS}, it becomes possible to calculate a realistic value for EF_{app}. However, calculating the average interfacial enhancement, EF_{int}, also requires that we know the decay length of enhancement, δ, in order to establish the thickness of the interfacial layer being probed. To measure δ, we prepared a set of samples with the configuration Q/Ag/PEDOT:PSS/P3HT, such that the distance between the Ag surface and a probe layer of conjugated polymer P3HT could be controlled by varying the thickness of the spacer layer from 2.2 to 41 nm. Poly(3,4-ethylenedioxythiophene):polystyrenesulfonate (PEDOT:PSS) was used for the spacer layer due to its low surface roughness, good transmittance, and small Raman scattering cross-section relative to P3HT. AFM revealed that increasing spacer thickness led to a lower surface roughness and a gradual blurring of the Ag surface features underneath (see Figure 2a,b).

For a sample with no PEDOT:PSS spacer layer (an effective Ag−P3HT separation of 0 nm), there was a large difference in scattered intensity from P3HT between normal Raman and SERS conditions (see Figure 2c). The integrated intensity of the C═C vibrational mode at ∼1450 cm^{-1} was 6.04 × 10^5 counts in the absence of Ag and 1.04 × 10^7 counts in the presence of Ag, leading to a calculated EF_{app} of 17.3 ± 2.6 for that mode. With the introduction of a 4.8 nm thick PEDOT:PSS spacer layer, the Raman intensity was unchanged but the SERS intensity was reduced to 2.13 × 10^6 counts, lowering the EF to 3.5 ± 0.16. A thicker spacer layer of 8.6 nm reduced the SERS intensity even further, with an EF of only 0.92 ± 0.15, indicative of no surface enhancement beyond ∼9 nm from the metal surface. A more accurate estimation, based on linear fitting of EF values for 11 samples with different spacer thicknesses (see Figure 3), found the decay length of

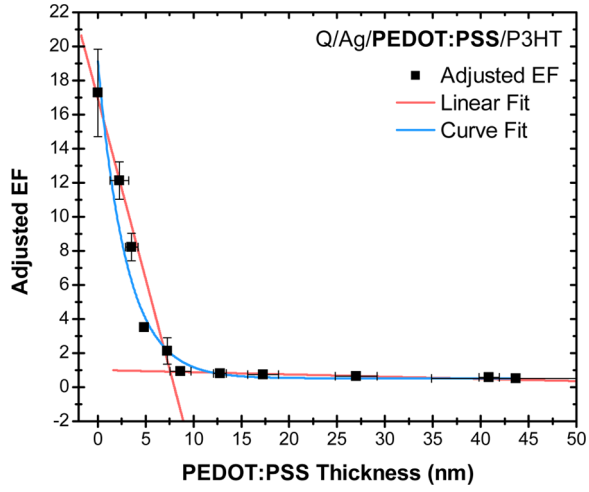

Figure 3. EF values for a ∼10 nm thick layer of P3HT plotted against thickness of a PEDOT:PSS spacer layer, with fitting to determine the decay length δ = 7.6 nm.

enhancement δ = 7.6 ± 0.2 nm. This compares well to values reported in the literature for general SERS applications and represents a significantly more accurate estimation than has been previously reported for SERS of conjugated polymer systems (<20 nm).[20]

We noted that between Raman and SERS spectra, there was a shift of the C═C peak toward higher wavenumbers, a shift that was only apparent when the separation was small enough for surface enhancement of P3HT (see insets of Figure 2c). For the first sample, where the spacer layer thickness was 0 nm, the peak was up-shifted from 1454 to 1460 cm^{-1} under SERS conditions, as the spacer thickness increased up to δ = 7.6 nm,

DOI: 10.1021/acsami.6b12124
ACS Appl. Mater. Interfaces 2016, 8, 31469−31481

the upshift reduced to zero and a consistent C═C peak position of 1452 cm^{-1}. The change closely matches what we reported previously for P3HT of low molecular order, where a shift of the C═C peak toward higher wavenumbers is due to a more twisted conformation of the conjugated backbone and results in a greater localization of π-electron density and a higher vibrational frequency.[6,26] We conclude that the SERS is selectively probing an interface dominated by conformational disorder, where confinement in proximity to a rough surface disrupts the organization of P3HT chains, as has been reported before.[27]

Having estimated δ, it becomes possible to calculate our representative value, the average interfacial enhancement factor EF_{int}, for organic films relevant to OPV manufacture, and compare values between films prepared under different fabrication conditions. To test the reliability of our model, Q/Ag/P3HT samples were prepared with a wide range of P3HT film thicknesses, from 3.0 to 85 nm. Raman and SERS spectra were taken, and EF_{app} was calculated from the integrated intensities of the C═C peak at 1450 cm^{-1} (see Figure 4a). EF_{app} appeared to follow an exponential decay curve, starting at 119 for the 3.0 nm thick film and decreasing rapidly toward an asymptotic value of 9.0 for the thickest films (>20 nm). This can be understood as a consequence of increasing dominance of scattering from the unenhanced portion (I_{bulk}) of thicker films.

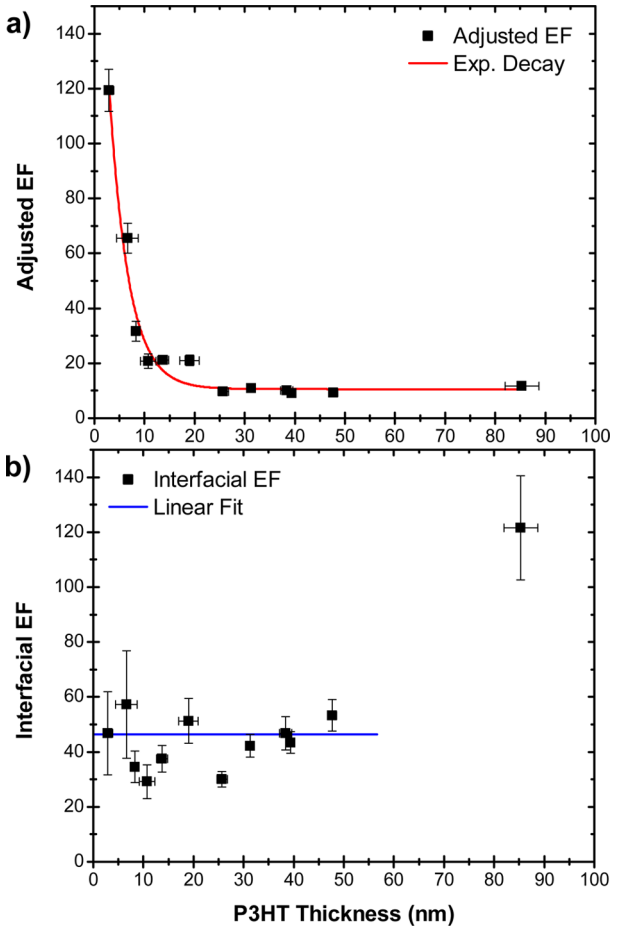

Figure 4. (a) Apparent EF for P3HT layers of varying thickness deposited on Ag, after adjusting for transmittance losses, and (b) interfacial EF calculated using eq 2.

Apparent EF values were then corrected for thickness to calculate EF_{int}, using eq 2 and δ = 7.6 nm, and plotted in Figure 4. For P3HT films with thicknesses of up to 50 nm, the calculated EF_{int} values ranged between 30 and 60, resulting in an average EF_{int} of 46.5 ± 9.3. This is a reasonable match to the apparent EF for $L = \delta$ predicted by the exponential decay curve, and although the variation around the average was significant and semiperiodic, it is worth noting that the average fell within the margin of error for approximately half of the calculated EF_{int} values. A single outlier was observed: the thickest film (85 nm) exhibited a much higher EF_{int} of 122. This outlier, and the semiperiodic variation in EF_{int}, suggest that there may be an additional thickness-related optical effect we have not accounted for, such as optical absorption by the film or optical interference from the multilayered sample structure. Modeling suggests that the predicted impact of absorption on intensities is insufficient to explain the oscillation in EF_{int} or the outlier at 85 nm, leading us to suspect that optical interference from each sample's many different layers is altering the electromagnetic field distribution within the thin film, becoming increasingly significant with film thickness. Thus, applying this technique to thicker films will require significant analysis of potential photonic structure within each sample via numerical simulations. To minimize the impact of these effects, all further films examined as part of this work were prepared with thicknesses of <80 nm.

In general, the model appears to work. Despite the apparent EF varying by an order of magnitude between samples of different film thicknesses, the correction led to most EF_{int} values being within a margin of error of the expected value. Despite certain limitations, which will require a more detailed analysis to be accounted for, it should be possible to apply this model to real material systems in order to permit the comparison of EF across different samples and architectures.

Having established a methodology for using SERS to reliably probe interfacial properties in organic thin films containing a single material, we then considered how it could be applied to the study of interfacial composition in blend films used for OPVs, which will have a disproportionate impact on the efficiency of charge extraction from the active layer and therefore influence the overall performance of the solar cell. Provided that the constituent materials (A and B) both produce Raman scattering and can be detected simultaneously, the relative concentration of each material can be determined from the composite Raman spectrum of the blend as follows:

$$\frac{N_A}{N_B} = \frac{\alpha}{\beta}\frac{\sigma_B}{\sigma_A} \quad (3)$$

where N is the relative concentration of each material, α and β are the intensities contributed to the overall Raman spectrum by A and B, respectively, and σ_B/σ_A is the relative Raman scattering cross-section of B with respect to A. α and β can be determined by deconvolution of the blend spectrum, using the spectra from the appropriate neat films.[8] Provided that α, β and σ_B/σ_A are known, the composition N_A/N_B can be calculated for any blend. For a spectrum taken under normal Raman conditions, the composition will be that of the bulk film, whereas under SERS conditions it will be that of the interface.

The chosen blend system was that of the two semiconducting polymers P3HT and F8TBT, deposited from *p*-xylene with a blend weight ratio of 1:1 in order to follow a previously reported protocol.[23] Samples of both the neat

DOI: 10.1021/acsami.6b12124
ACS Appl. Mater. Interfaces 2016, 8, 31469−31481

materials and the blend were prepared with two different sample configurations: top-contact (Q/organic/Ag) and bottom-contact (Q/Ag/organic), in order to investigate top and bottom interfaces separately. In accordance with previous reports of device performance for this blend system, we also compared the properties of as-cast films with those thermally annealed at 140 °C. As annealing after evaporation of the metallic top electrode has been reported to improve device performance more than preannealing,[23] top-contact samples were either pre- or postannealed in order to identify any changes in composition at the top interface that might be responsible.

First, we examined the properties of the two polymers in neat films, in order to identify any spectral variations that may result from changes in bulk (Raman) or interface (SERS) morphology as a result of annealing; and develop an understanding of how these materials behave under surface enhancement in each of the five sample configurations. The normalized Raman spectra for neat P3HT (Figure 5) were

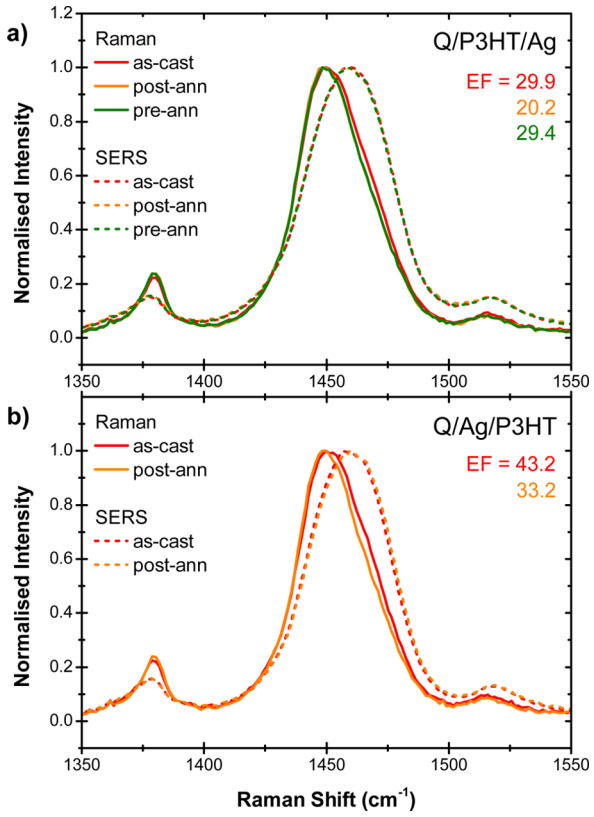

Figure 5. Normalized Raman and SERS spectra for films of neat P3HT in top-contact (a) and bottom-contact (b) sample configurations.

identical for both top-contact and bottom-contact sample configurations, exhibiting C=C peaks positioned at 1450 cm^{-1} with fwhm of 36 cm^{-1}. As was described earlier, the peak position and fwhm of the P3HT C=C mode are sensitive to backbone planarity (i.e., molecular order) and, using our previously reported method of deconvolution,[8] the degree of molecular order was calculated to be 0.95, with respect to a pure regioregular-P3HT (RR-P3HT) reference sample with maximized molecular order.[26] After thermal annealing, the C=C peak was slightly downshifted (to 1449 cm^{-1}) and narrower (by 2 cm^{-1}), resulting in a slightly higher molecular order (1.0) achieved when the polymer reorganizes at high temperatures, making it morphologically equivalent to the RR-P3HT reference sample used for deconvolution.[8,26] The similarity between Raman measurements of top-contact and bottom-contact samples is due to the fact that in the absence of the Ag layer, the samples are effectively identical (Q/organic) and have the same bulk properties.

When the neat P3HT samples were probed under SERS conditions, they all exhibited a more disordered spectrum, as indicated by a broader C=C peak shifted to higher wavenumbers (see Figure 5, or Supporting Information for individual spectra).[26] The top-contact sample exhibited marginally more disorder than the bottom-contact sample: having a C=C peak position of 1461 cm^{-1} compared to 1457 cm^{-1}, and fwhm of 41 cm^{-1} vs 40 cm^{-1}, and the degree of molecular order was calculated to be 0.68 at the top interface and 0.69 at the bottom interface. As noted earlier, this reveals that both interfaces are significantly more disordered than the bulk film when in proximity to a metal surface. Slightly greater disorder at the top interface could be considered evidence that the thermal evaporation of Ag atoms onto the organic film damages it or otherwise alters its morphology, but the variation was within the error of our calculation method (±0.02). Thermal annealing led to a consistent C=C peak position of 1460 cm^{-1} (and molecular order of ~0.65), independent of whether the film was pre- or postannealed.

In terms of enhancement, there was a striking difference in the enhancement observed at the top and bottom interfaces of the as-cast film, which gave interfacial enhancement factors of 29.9 and 43.2, respectively. The latter is a good match for the average EF_{int} of 46.5 that was obtained earlier for P3HT in the same configuration (Figure 4b), and provides some indication that the model can effectively compare sample sets across different evaporation batches. The difference in EF between top and bottom interfaces is unexpected, but we propose that it arises from a better wetting between the layers obtained when the polymer is deposited directly onto Ag, versus when the Ag is evaporated onto the polymer. After postannealing, the magnitude of enhancement was reduced at both interfaces, with EF decreasing from 29.9 to 20.2 at the top interface, and from 43.2 to 33.2 at the bottom interface. No such change was observed at the top interface after preannealing, which gave an EF of 29.4, close to the original top interface value. Evidently, there is some form of structural change at the Ag interface that reduces EF during postannealing. We noted earlier that thermally annealing the Ag layer leads to a red-shift in plasmon resonance frequency, but as the decrease in EF was not observed for F8TBT samples prepared using Ag layers from the same evaporation (see Figure 6), we have to conclude that it is specific to the interaction of Ag and P3HT at both interfaces.

When samples of neat F8TBT were examined under normal Raman conditions, they exhibited a complex Raman spectrum with several peaks between 1250 and 1600 cm^{-1} (see Figure 6a). Six major modes were identified and assigned using DFT simulations to specific C−C and C=C symmetric stretching vibrations of the fluorene, thiophene, and benzothiadiazole moieties (herein referred to as F, T, and BT) that comprise the polymer's repeat unit (see Supporting Information for DFT simulations). The major peaks were numbered from low to high Raman shift, with four representing vibrations of single units: Peak 1 (1270 cm^{-1}) was the benzene C−H waggling mode of the F unit, Peak 4 (1448 cm^{-1}) was the C=C stretching mode of the T unit, Peak 5 (1536 cm^{-1}) was the

DOI: 10.1021/acsami.6b12124
ACS Appl. Mater. Interfaces 2016, 8, 31469−31481

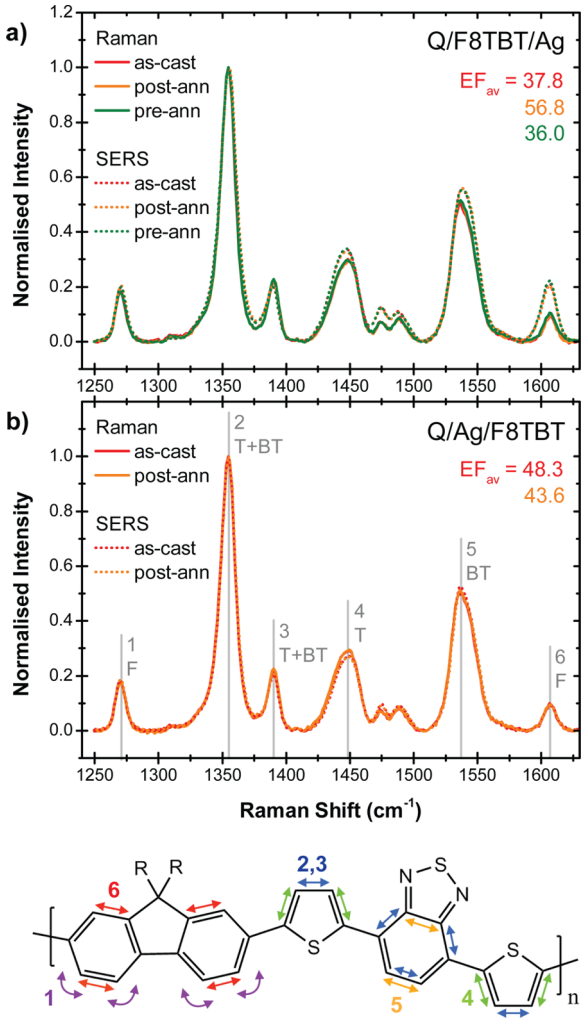

Figure 6. Normalized Raman and SERS spectra for films of neat F8TBT in top-contact (a) and bottom-contact (b) sample configurations, including vibrational mode assignments to particular monomer units.

benzene ring stretching mode of the BT unit, and Peak 6 (1608 cm^{-1}) was the benzene quadrant stretching mode of the F unit. The remaining peaks were assigned to coupled vibrations of the T and BT units: Peak 2 (1355 cm^{-1}) and Peak 3 (1390 cm^{-1}) were, respectively, the symmetric and antisymmetric forms of the C═C mode of the BT unit coupled to the C−C mode of the T unit. The vibrations of the T and BT (acceptor) units appear the strongest, whereas vibrations of the F (donor) unit are weakest, because the chosen excitation wavelength (488 nm) was resonant with the charge-transfer absorption transition (see Supporting Information).

When F8TBT films with different sample configurations were compared, they were found to exhibit identical spectra under normal Raman conditions. As with P3HT, the similarity between top- and bottom-contact samples agrees with our expectation there should be no variation in the as-cast bulk film between the two basic sample configurations in the absence of Ag. However, unlike P3HT, thermal annealing evidently has no strong impact on the vibrational frequencies or relative intensities of the Raman modes for bulk F8TBT. When Raman and SERS spectra were compared for each sample configuration (see Figure 6), there was a clear difference between top- and bottom-contact sample configurations. Under SERS conditions, the spectra from top-contact samples were altered slightly compared to normal Raman: although there were no meaningful changes in peak position, there was an increase in the relative intensities of Peaks 4, 5, and 6 (at 1448, 1536, and 1608 cm^{-1}, respectively) with respect to Peak 2 (at 1355 cm^{-1}). This was not apparent for either the as-cast or postannealed bottom-contact samples, and therefore, it was particular to the top interface of the neat F8TBT film. Furthermore, the change in relative intensity was observed for all top-contact samples, whether as-cast, postannealed, or preannealed.

Interfacial EF values were then calculated for each F8TBT peak separately and plotted in Figure 6. At the bottom interface, the average EF for Peaks 1−5 was 48.3, whereas at the top interface, it was 37.8. The higher EF at the bottom interface agrees well with what was observed for neat P3HT and further reinforces our proposed explanation that enhancement is inherently stronger at the bottom Ag/organic interface rather than being specific to a particular organic material. Peak 6 was a major exception to this rule, however: the greater relative intensity of this mode under SERS conditions at the top interface only (as shown in Figure 6) means the peak also has a correspondingly larger EF of 97, compared to 49 for bottom-contact. The reason for the selective enhancement of Peak 6 at 1606 cm^{-1} lies in its assignment to a vibrational mode of the F unit, as the relative intensity of the F unit's vibration in a similar polymer (F8BT) has been reported to depend strongly on the torsion angle between the F and BT units.[27] A larger I_{BT}/I_F ratio at the bottom interface is indicative of a smaller torsion angle and greater π-electron delocalization along the chain. However, in the case of F8BT, a larger torsion angle is associated with better intermolecular electron transport, as it forces neighboring chains to stack cofacially, with better overlap between the lowest unoccupied molecular orbitals (LUMOs) of adjacent BT units.[28] DFT simulations have shown that the same relationship between torsion angle and I_{BT}/I_F applies to F8TBT (see Supporting Information).

Under normal Raman conditions, all neat films exhibited a similar I_{BT}/I_F ratio of 10 ± 0.3, indicating a similar T-BT torsion angle, and thus, a similar degree of planarity is adopted by the polymer in the bulk of both as-cast and annealed films. Under SERS conditions, the as-cast top- and bottom-contact samples exhibited I_{BT}/I_F ratios of 4.4 and 11.1, respectively. This suggests F8TBT adopts a much larger F−BT torsion angle at the top interface and slightly smaller angle at the bottom interface, compared to the average angle in the bulk of the film. If F8TBT exhibits superior electron transport when twisted, as reported for F8BT, this arrangement would better suit inverted devices where electrons are extracted from the top interface, provided that the same pattern of interfacial torsion angles is retained by F8TBT when it is blended with P3HT.

For the top-contact sample in Figure 6a, postannealing resulted in much stronger enhancement of all peaks: the average EF of Peaks 1−5 rose by 50% from 37.8 to 56.8. Interestingly, Peak 6 exhibited the smallest improvement in EF (38%), and there was a corresponding increase in I_{BT}/I_F ratio from 4.3 to 4.5. This indicates that a slightly more planar F-BT conformation is adopted at the top interface when annealed in the presence of a capping Ag layer, though the variation was very close to the estimated ratio measurement error of ±0.1. The opposite effect was observed for the bottom-contact sample, as postannealing reduced the average EF for Peaks 1−5 by 9.5% from 48.27 to 43.6. There was still an increase in the

DOI: 10.1021/acsami.6b12124
ACS Appl. Mater. Interfaces 2016, 8, 31469−31481

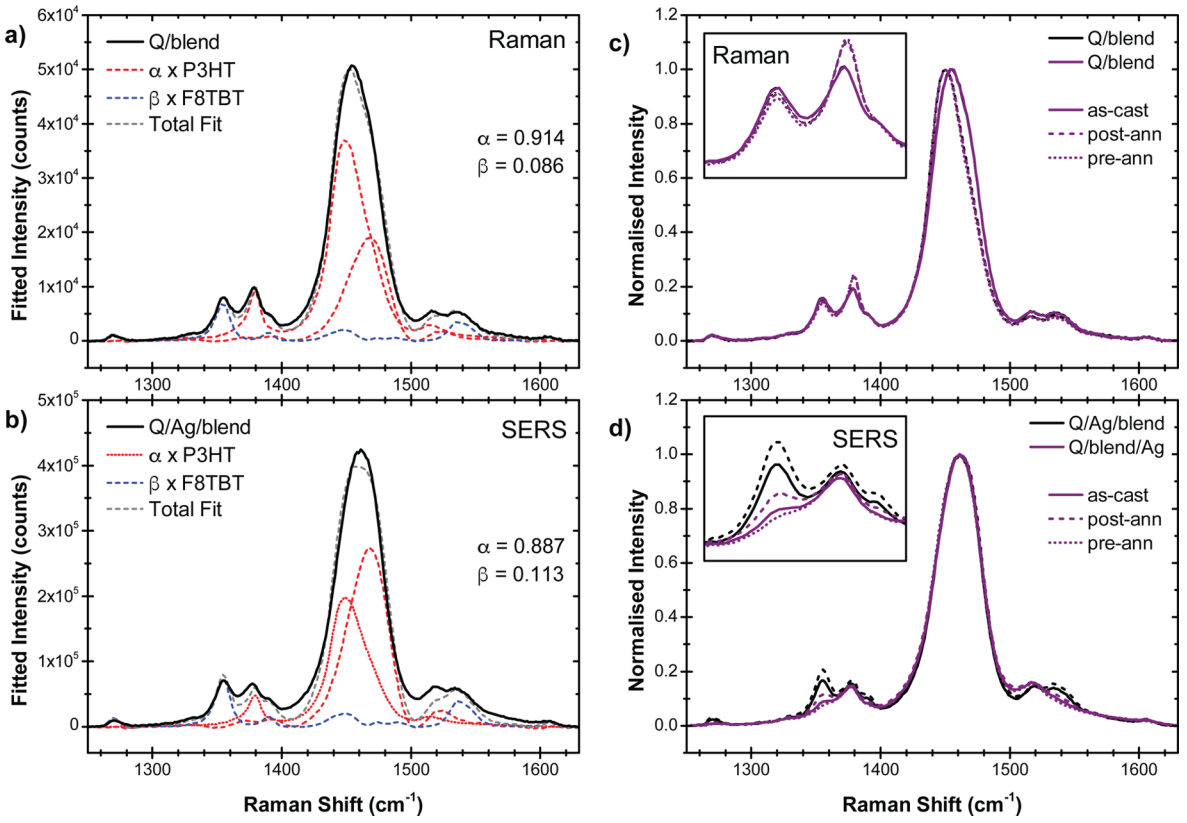

Figure 7. Raman (a) and SERS (b) spectra for an as-cast sample of Q/Ag/P3HT:F8TBT, fitted using RR-P3HT (as ordered fraction), RRa-P3HT (as disordered fraction) and F8TBT spectra to obtain relative contributions of P3HT (α) and F8TBT (β). Normalized Raman (c) and SERS (d) spectra for P3HT:F8TBT blends in five different sample configurations, with variation in the relative intensity of the F8TBT peak at 1356 cm^{-1} shown in each inset.

I_{BT}/I_F ratio, from 10.2 to 10.5, suggesting the adoption of a slightly less planar conformation at the bottom interface after annealing, but the difference in ratio was well within the estimated error of ±1.0 for those samples. Thus, it seems that postannealing has little effect on the difference in F−BT torsion angle and chain planarity between the more planar top interface and the less planar bottom interface, according to their I_{BT}/I_F ratios of 4.5 and 10.5, respectively. Preannealing was expected to have little effect on EF at the top interface, as was shown previously with P3HT. However, there was a slight decrease in overall EF for F8TBT, with values for Peaks 1−5 reduced by 0−7%, which may relate to a change in surface roughness at the interface. There was also no meaningful change in the I_{BT}/I_F ratio, remaining at 4.3 ± 0.1, indicating a consistent F−BT torsion angle. In summary, it appears that while postannealing acted to very slightly increase the planarity of F8TBT chains at the top interface, preannealing had no effect. In any case, the changes observed were so small that there would be correspondingly little impact on charge transport/extraction properties at that interface.

Having obtained both Raman and SERS spectra for the neat materials in all sample configurations, it was possible to study the blend spectrum and deconvolute it to obtain the intensity values α and β, essential to calculating composition. First, we examined the spectrum of an as-cast bottom-contact sample (Q/Ag/blend) under normal Raman conditions, which was composed of overlapping peaks from P3HT (at 1379 and 1454 cm^{-1}) and from F8TBT (at 1354 and 1536 cm^{-1}), as shown in Figure 7a. The remaining peaks of F8TBT were not apparent due to overlap with P3HT, and despite the fact that blend film was prepared with a weight ratio of 1:1, there is a clear disparity in the Raman intensities produced by the two materials, with the blend spectrum almost completely dominated by P3HT. Deconvolution gives a more quantitative value: the fitted intensities for P3HT and F8TBT were found to be α = 0.914 and β = 0.086, respectively, expressed as fractions of the total Raman intensity. The explanation for this lies in the relative magnitude of their Raman scattering cross sections σ, which determine how likely it is that a given molecule will scatter an incident photon inelastically (i.e., contribute to the Raman spectrum). Using the known weight ratio of the blend and rearranging eq 3, we can calculate the relative Raman scattering cross sections at this wavelength from the fitted intensities. For the as-cast blend shown in Figure 7a, we calculate that the cross-section for F8TBT is 0.094 ± 0.012, relative to that of P3HT. A ∼10-fold difference in cross-section is not particularly surprising; under resonant conditions P3HT has consistently been one of the most strongly Raman-active molecules we have explored in our investigations of organic semiconducting materials, and many other materials are almost undetectable when blended with P3HT, including polymers such as DPP-TT-T and PTB7, and the fullerenes $PC_{60}BM$ and $PC_{70}BM$.[6,8,9]

Taking the average value across all five sample configurations to be representative of the relative cross-section of F8TBT to P3HT (0.102 ± 0.008), it becomes possible to calculate the composition of any given blend film using the fitted intensities α and β, and eq 3. When the SERS spectrum of the same sample (Q/Ag/blend) was deconvoluted, an increase in the fitted intensity of F8TBT was observed, from 0.086 to 0.113, that suggests a greater concentration of F8TBT at the bottom

DOI: 10.1021/acsami.6b12124
ACS Appl. Mater. Interfaces 2016, 8, 31469−31481

interface. After accounting for the difference in cross-sections between the two polymers, we found that the composition of the bottom interface was slightly F8TBT-rich, consisting of 44.5% P3HT and 55.5% F8TBT.

The best fit was obtained with the P3HT contribution divided into ordered and disordered components (using regioregular-P3HT and regiorandom-P3HT spectra as references for order and disorder, respectively) that were allowed to vary separately, as shown in Figure 7a. This meant that any variations in molecular order within the blend could be measured, and we note the as-cast blend exhibited a slightly lower degree of molecular order in the bulk compared to neat P3HT, 0.79 versus 0.95, respectively, which shifted the C═C peak to 1454 cm^{-1} and can be attributed to reduced crystallinity when intermixed with F8TBT. Under SERS conditions, fitting revealed a markedly larger fraction of disordered P3HT (see Figure 7b), which further shifted the C═C peak from 1454 to 1461 cm^{-1} and reduced the estimated degree of molecular order from 0.79 to 0.60. This follows the behavior observed for neat P3HT under SERS conditions (which exhibited a C═C peak at 1457 cm^{-1}), and similarly, we consider SERS to be selectively probing a very disordered interfacial morphology. The quality of the fit was somewhat lower for the SERS spectrum due to the lower degree of P3HT molecular order, a limitation for the deconvolution method due to using references that represent the extremes of maximum and minimum order. However, the resulting errors remain quite low, and we still consider fitting to be representative of the actual components in both Raman and SERS.

The Raman and SERS spectra for the blend films in all five sample configurations are plotted in Figures 7c,d, and the insets demonstrate that under Raman conditions there were some differences in Raman spectra that indicate changes in bulk morphology. These changes were not of composition, there was little variation in the relative intensities of F8TBT and P3HT measured by Raman, due to the bulk film having the same weight ratio of the two polymers regardless of configuration or annealing, but instead, the variation was in terms of P3HT molecular order. Thermal annealing was found to have a profound impact on P3HT in the blend: shifting the P3HT C═C peak to lower wavenumbers (~1450 cm^{-1}) and a narrower fwhm (~37 cm^{-1}). Postannealing increased the estimated degree of molecular order from 0.79 to 0.94, while preannealing increased it to 0.95, both resulting in deconvoluted P3HT spectra effectively equivalent to the neat polymer. We conclude that thermal annealing has acted to increase phase separation between P3HT and F8TBT in the bulk of the blend, leading to purer P3HT domains of greater molecular order as has been observed similarly for P3HT:PCBM blends.[6]

While this phase separation is certainly taking place in the bulk of the film, normal Raman cannot tell us whether annealing affects interfacial composition in the same way. Under SERS conditions (Figure 7d), there was no apparent variation in the C═C peak of P3HT, which all exhibited the same peak position (~1461 cm^{-1}) and fwhm (~41 cm^{-1}) indicative of significantly disordered P3HT (a degree of molecular order of ~0.60). However, there was a large variation in the relative intensities of F8TBT and P3HT, demonstrated by the F8TBT mode at ~1359 cm^{-1} shown in the inset of Figure 7d, that was not observed under normal Raman conditions. Evidently SERS is probing different interfacial compositions in each sample configuration, with the clearest contrast appearing between top and bottom interfaces. After deconvolution to obtain fitted intensities α and β, interfacial compositions were calculated and tabulated in Table 1, along with the average EF measured separately for each material.

Table 1. Deconvoluted EF_{int} Values and Interfacial Compositions for P3HT:F8TBT Blend Films in Five Different Sample Configurations, According to SERS

sample	EF_{P3HT}	EF_{F8TBT}	% P3HT	% F8TBT
Q/blend/Ag	49.7	12.1	74.5	25.5
Q/blend/Ag postann	37.3	13.1	65.2	34.8
Q/blend/Ag preann	55.1	5.0	83.3	16.7
Q/Ag/blend	57.4	72.0	44.5	55.5
Q/Ag/blend postann	51.4	76.2	38.4	61.6

The relative enhancement of F8TBT was found to be significantly higher in the as-cast bottom-contact sample (Q/Ag/blend) compared to the top-contact sample (Q/blend/Ag), resulting in a composition of 55.5% F8TBT at the bottom interface and only 25.5% F8TBT at the top interface. Immediately, this seems to indicate that the P3HT:F8TBT blend is, morphologically speaking, better suited to inverted device architectures, with electrons extracted from F8TBT at the bottom interface and holes extracted from P3HT at the top interface. This agrees with the conclusions of Sepe et al., who measured interfacial composition using XPS and UPS and observed a P3HT-rich capping layer at the top surface of these blends, but not with their observation that there was no F8TBT-rich wetting layer at the bottom of the blend.[29] However, an interfacial composition that varies by only 5% from that of the bulk may not have been detectable using other techniques. Furthermore, the direction of separation follows our understanding that during deposition from solution, the high-surface-energy material will be preferentially attracted to the high-surface-energy (substrate) interface, while the low-surface-energy material is preferentially attracted to the low surface energy (air) interface, as has been shown for other blend systems, including P3HT:PCBM and TFB:F8BT.[12,15] By this reasoning, we conclude that F8TBT is the high-surface-energy material, as has been reported for F8BT, whereas P3HT is low-surface-energy material, leading to the distribution of material illustrated in Figure 8.

Thermal annealing was found to have a very significant impact on interfacial composition, and depended strongly on the timing of the anneal (pre- vs postannealing). When the bottom-contact sample was postannealed, it resulted in a more selective enhancement of F8TBT compared to the as-cast sample, and the F8TBT content at the bottom interface was determined to have increased from 55.5% to 61.6%. This was consistent with greater vertical phase separation of the film and agreed with earlier observations that annealing leads to greater phase separation and improved P3HT molecular order in the bulk blend. When the top-contact sample was postannealed, there was a similarly greater enhancement of F8TBT, indicating a higher F8TBT content at the top interface, which had increased from 25.5% to 34.5%. Evidently there is a preferential diffusion of F8TBT toward the Ag interface during thermal annealing, whether it is at the top of the film or the bottom, which may be attributed to its high surface energy (see Figure 8). This was confirmed by examining the preannealed film: weaker enhancement of F8TBT and stronger enhancement of P3HT revealed that, when annealed in the absence of Ag, the

DOI: 10.1021/acsami.6b12124
ACS Appl. Mater. Interfaces 2016, 8, 31469−31481

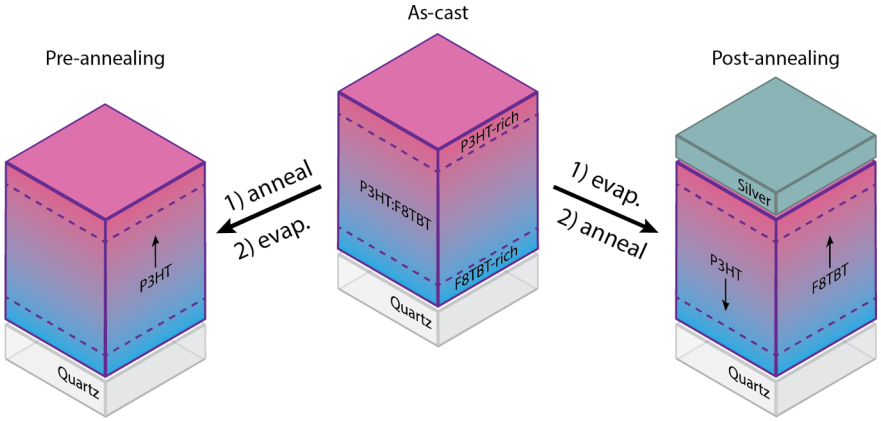

Figure 8. Illustration of the distribution of material that forms during deposition of an as-cast blend, and how the distribution of material changes during thermal annealing before vs after evaporation of a capping silver electrode (pre- vs postannealing).

F8TBT content of the top interface is reduced (decreasing from 25.5% to 16.7%). This can be understood as a preferential diffusion of P3HT rather than F8TBT toward the top of the film, due to its nature as a low-energy air interface during preannealing (see Figure 8).

Clearly, there is a significant difference between interfacial composition and the bulk, and those interfaces, which are rich in a particular material, will have a profound impact on the efficiency of charge extraction from the blend film in devices such as OPVs. Furthermore, the use of thermal annealing to modify bulk properties (such as phase separation) will also influence interfacial properties, depending on the surface energy at the top and bottom of the film during annealing.

CONCLUSIONS

SERS is a powerful technique that has been used extensively in several other research fields, and offers the same potential selectivity and vertical resolution to the study of organic thin films. We have demonstrated a thorough, quantitative method of applying SERS to the study of interfacial properties in organic thin films. By exploiting the distance dependence of a plasmonic field, the diffraction limit for optical techniques such as Raman spectroscopy can be circumvented, and detailed information on chemical structure, morphology, and composition can be obtained for only those molecules within a few nanometers of a metal substrate. By understanding interfacial properties, particularly composition in blends, we can better interpret how morphology influences the performance of electronic devices based on organic semiconductors, such as charge extraction from organic solar cells. We have shown that it was relatively simple to produce plasmonically active metal surfaces through the thermal evaporation of ultrathin (~7 nm) silver layers, with strong plasmonic resonance in the visible spectrum suitable for resonance with a broad range of excitation wavelengths. These layers provided relatively low surface enhancement factors, with single molecule EFs estimated to be at least 450×, but more importantly were compatible with organic thin films and displayed a strong distance dependence of enhancement, probing only those molecules within ~7.6 nm of the metal surface.

On the basis of the evidence SERS provides regarding interfacial properties of the polymer:polymer blend P3HT:F8TBT, we conclude that the blend naturally forms two interfacial layers during deposition, with a capping layer very rich in P3HT at the top of the film and a wetting layer slightly rich in F8TBT at the bottom of the film. Such a distribution of material is expected to better suit inverted device architectures, where electrons are extracted from F8TBT at the bottom of the active layer and holes are extracted from P3HT at the top. It was possible to modify the interfacial compositions through thermal annealing, but it strongly depended on whether the film was annealed before or after evaporation of the metallic top-contact, which significantly changes the surface energy of the top interface. Preannealing increased the concentration of low-surface-energy P3HT at that top interface, whereas postannealing raised the concentration of high-surface-energy F8TBT. Consequently, postannealing is expected to improve electron extraction from F8TBT at the top interface and make the blend better suited to conventional device architectures, in good agreement with the reported improvement in device performance for P3HT:F8TBT solar cells after postannealing compared to preannealing.[23]

With further development of this methodology, SERS has the potential to be applied to the investigation of an even broader range of interfacial properties key to device performance, including molecular orientation, that are detectable to a versatile technique like Raman spectroscopy. Additionally, the methods described here could be used with an even more advanced technique, tip-enhanced raman spectroscopy (TERS), to quantitatively study interfacial properties with nanometer resolution in both lateral and vertical directions.

ASSOCIATED CONTENT

Supporting Information

The Supporting Information is available free of charge on the ACS Publications website at DOI: 10.1021/acsami.6b12124.

Detailed description of methodology for transmittance correction of Raman/SERS intensities, derivation of interfacial model (eq 2), figures for batch-to-batch variation in Ag properties, individual Raman/SERS spectra for neat P3HT, neat F8TBT and blended P3HT:F8TBT, DFT simulations of F8TBT oligomers with effect of torsion on predicted Raman spectra (PDF)

AUTHOR INFORMATION

Corresponding Author

*E-mail: ji-seon.kim@ic.ac.uk.

DOI: 10.1021/acsami.6b12124
ACS Appl. Mater. Interfaces 2016, 8, 31469−31481

Author Contributions

The manuscript was written through contributions of all authors. All authors have given approval to the final version of the manuscript.

Notes

The authors declare no competing financial interest.

■ ACKNOWLEDGMENTS

This work was funded by the EPSRC through the Plastic Electronics Doctoral Training Centre (EP/G037515/1). We also acknowledge EPSRC support from EP/K029843/1, Cambridge Display Technology (CDT) CASE studentship and Samsung GRO program. The authors would also like to acknowledge Welsh Assembly Government funded Ser Cymru Solar Project.

■ ABBREVIATIONS

OPV = organic photovoltaics
OLED = organic light-emitting diode
SERS = surface-enhanced Raman spectroscopy
P3HT = poly(3-hexylthiophene)
F8TBT = poly((9,9-dioctylfluorene)-2,7-diyl-*alt*-[4,7-bis(3-hexylthien-5-yl)-2,1,3-benzothiadiazole]-2′,2″-diyl)
AFM = atomic force microscopy
EF = enhancement factor
smEF = single-molecule enhancement factor
EF_{app} = apparent enhancement factor
EF_{int} = interfacial enhancement factor
I_{RS} = Raman intensity
I_{SERS} = surface-enhanced Raman intensity

■ REFERENCES

(1) Nelson, J.; Emmott, C. J. M. Can Solar Power Deliver? *Philos. Trans. R. Soc., A* **2013**, *371* (1996), 20120372−20120372.
(2) Azzopardi, B.; Emmott, C. J. M.; Urbina, A.; Krebs, F. C.; Mutale, J.; Nelson, J. Economic Assessment of Solar Electricity Production from Organic-Based Photovoltaic Modules in a Domestic Environment. *Energy Environ. Sci.* **2011**, *4* (10), 3741−3753.
(3) James, D. T.; Kjellander, B. K. C.; Smaal, W. T. T.; Gelinck, G. H.; Combe, C.; McCulloch, I.; Wilson, R.; Burroughes, J. H.; Bradley, D. D. C.; Kim, J. S. Thin-Film Morphology of Inkjet-Printed Single-Droplet Organic Transistors Using Polarized Raman Spectroscopy: Effect of Blending TIPS-Pentacene with Insulating Polymer. *ACS Nano* **2011**, *5* (12), 9824−9835.
(4) Spanggaard, H.; Krebs, F. C. A Brief History of the Development of Organic and Polymeric Photovoltaics. *Sol. Energy Mater. Sol. Cells* **2004**, *83* (2−3), 125−146.
(5) National Renewable Energy Laboratory. NREL Best Research Cell Efficiencies Chart, 2015. Available at the following: http://www.nrel.gov/ncpv/images/efficiency_chart.jpg.
(6) Hoppe, H.; Niggemann, M.; Winder, C.; Kraut, J.; Hiesgen, R.; Hinsch, A.; Meissner, D.; Sariciftci, N. S. Nanoscale Morphology of Conjugated Polymer/Fullerene-Based Bulk- Heterojunction Solar Cells. *Adv. Funct. Mater.* **2004**, *14* (10), 1005−1011.
(7) Westacott, P.; Tumbleston, J. R.; Shoaee, S.; Fearn, S.; Bannock, J. H.; Gilchrist, J. B.; Heutz, S.; DeMello, J.; Heeney, M.; Ade, H.; Durrant, J.; McPhail, D. S.; Stingelin, N. On the Role of Intermixed Phases in Organic Photovoltaic Blends. *Energy Environ. Sci.* **2013**, *6*, 2756−2764.
(8) Razzell-Hollis, J.; Limbu, S.; Kim, J.-S. Spectroscopic Investigations of Three-Phase Morphology Evolution in Polymer: Fullerene Solar Cell Blends. *J. Phys. Chem. C* **2016**, *120* (20), 10806−10814.
(9) Tsoi, W. C.; Zhang, W.; Razzell Hollis, J.; Suh, M.; Heeney, M.; McCulloch, I.; Kim, J.-S. In-Situ Monitoring of Molecular Vibrations of Two Organic Semiconductors in Photovoltaic Blends and Their Impact on Thin Film Morphology. *Appl. Phys. Lett.* **2013**, *102* (17), 173302.
(10) Parnell, A. J.; Dunbar, A. D. F.; Pearson, A. J.; Staniec, P. a; Dennison, A. J. C.; Hamamatsu, H.; Skoda, M. W. a; Lidzey, D. G.; Jones, R. a L. Depletion of PCBM at the Cathode Interface in P3HT/PCBM Thin Films as Quantified via Neutron Reflectivity Measurements. *Adv. Mater.* **2010**, *22* (22), 2444−2447.
(11) Sachs-Quintana, I. T.; Heumüller, T.; Mateker, W. R.; Orozco, D. E.; Cheacharoen, R.; Sweetnam, S.; Brabec, C. J.; McGehee, M. D. Electron Barrier Formation at the Organic-Back Contact Interface Is the First Step in Thermal Degradation of Polymer Solar Cells. *Adv. Funct. Mater.* **2014**, *24* (25), 3978−3985.
(12) Campoy-Quiles, M.; Ferenczi, T.; Agostinelli, T.; Etchegoin, P. G.; Kim, Y.; Anthopoulos, T. D.; Stavrinou, P. N.; Bradley, D. D. C.; Nelson, J. Morphology Evolution via Self-Organization and Lateral and Vertical Diffusion in Polymer:fullerene Solar Cell Blends. *Nat. Mater.* **2008**, *7* (2), 158−164.
(13) Bailey, J.; Wright, E. N.; Wang, X.; Walker, A. B.; Bradley, D. D. C.; Kim, J.-S. Understanding the Role of Ultra-Thin Polymeric Interlayers in Improving Efficiency of Polymer Light Emitting Diodes. *J. Appl. Phys.* **2014**, *115* (20), 204508.
(14) Kim, J.-S.; Friend, R. H.; Grizzi, I.; Burroughes, J. H. Spin-Cast Thin Semiconducting Polymer Interlayer for Improving Device Efficiency of Polymer Light-Emitting Diodes. *Appl. Phys. Lett.* **2005**, *87* (2), 023506.
(15) Kim, J.-S.; Ho, P. K. H.; Murphy, C. E.; Friend, R. H. Phase Separation in Polyfluorene-Based Conjugated Polymer Blends: Lateral and Vertical Analysis of Blend Spin-Cast Thin Films. *Macromolecules* **2004**, *37* (8), 2861−2871.
(16) Campion, A.; Kambhampati, P. Surface-Enhanced Raman Scattering. *Chem. Soc. Rev.* **1998**, *27*, 241−250.
(17) Lombardi, J. R.; Birke, R. L. A Unified Approach to Surface-Enhanced Raman Spectroscopy. *J. Phys. Chem. C* **2008**, *112* (14), 5605−5617.
(18) Moskovits, M. Surface-Enhanced Raman Spectroscopy: A Brief Retrospective. *J. Raman Spectrosc.* **2005**, *36* (6−7), 485−496.
(19) Wood, S.; Wade, J.; Shahid, M.; Collado-Fregoso, E.; Bradley, D. D. C.; Durrant, J. R.; Heeney, M.; Kim, J.-S. Natures of Optical Absorption Transitions and Excitation Energy Dependent Photostability of Diketopyrrolopyrrole (DPP)-Based Photovoltaic Copolymers. *Energy Environ. Sci.* **2015**, *8*, 3222−3232.
(20) Linde, S.; Carella, A.; Shikler, R. New Approach for Analyzing the Vertical Structure of Polymer Thin Films Based on Surface-Enhanced Raman Scattering. *Macromolecules* **2012**, *45* (3), 1476−1482.
(21) Baibarac, M.; Lapkowski, M.; Pron, A.; Lefrant, S.; Baltog, I. SERS Spectra of poly(3-Hexylthiophene) in Oxidized and Unoxidized States. *J. Raman Spectrosc.* **1998**, *29* (9), 825−832.
(22) Li, D.; Borys, N. J.; Lupton, J. M. Probing the Electrode-Polymer Interface in Conjugated Polymer Devices with Surface-Enhanced Raman Scattering. *Appl. Phys. Lett.* **2012**, *100* (14), 141907.
(23) McNeill, C. R.; Halls, J. J. M.; Wilson, R.; Whiting, G. L.; Berkebile, S.; Ramsey, M. G.; Friend, R. H.; Greenham, N. C. Efficient Polythiophene/Polyfluorene Copolymer Bulk Heterojunction Photovoltaic Devices: Device Physics and Annealing Effects. *Adv. Funct. Mater.* **2008**, *18* (16), 2309−2321.
(24) Le Ru, E. C.; Etchegoin, P. G. *Principles of Surface-Enhanced Raman Spectroscopy*; Elsevier B.V.: Amsterdam, The Netherlands, 2009.
(25) Watanabe, H.; Hayazawa, N.; Inouye, Y.; Kawata, S. DFT Vibrational Calculations of Rhodamine 6G Adsorbed on Silver: Analysis of Tip-Enhanced Raman Spectroscopy. *J. Phys. Chem. B* **2005**, *109*, 5012−5020.
(26) Tsoi, W. C.; James, D. T.; Kim, J. S.; Nicholson, P. G.; Murphy, C. E.; Bradley, D. D. C.; Nelson, J.; Kim, J.-S. The Nature of in-Plane Skeleton Raman Modes of P3HT and Their Correlation to the Degree of Molecular Order in P3HT:PCBM Blend Thin Films. *J. Am. Chem. Soc.* **2011**, *133* (25), 9834−9843.

DOI: 10.1021/acsami.6b12124
ACS Appl. Mater. Interfaces 2016, 8, 31469−31481

(27) Wood, S.; Franklin, J. B.; Stavrinou, P. N.; McLachlan, M. A.; Kim, J. Interfacial Molecular Order of Conjugated Polymer in P3HT: ZnO Bilayer Photovoltaics and Its Impact on Device Performance. *Appl. Phys. Lett.* **2013**, *103* (15), 153304.
(28) Donley, C. L.; Zaumseil, J.; Andreasen, J. W.; Nielsen, M. M.; Sirringhaus, H.; Friend, R. H.; Kim, J. Effects of Packing Structure on the Optoealectronic and Charge Transport Properties in poly(9,9-Di-N-Octylfluorene-Alt-Benzothiadiazole). *J. Am. Chem. Soc.* **2005**, *127* (37), 12890−12899.
(29) Sepe, A.; Rong, Z.; Sommer, M.; Vaynzof, Y.; Sheng, X.; Müller-Buschbaum, P.; Smilgies, D.-M.; Tan, Z.-K.; Yang, L.; Friend, R. H.; Steiner, U.; Hüttner, S. Structure Formation in P3HT/F8TBT Blends. *Energy Environ. Sci.* **2014**, *7* (5), 1725−1736.

DOI: 10.1021/acsami.6b12124
ACS Appl. Mater. Interfaces 2016, 8, 31469−31481